Computation of Radar Scattering From Heterogeneous Rough Soil Using the Finite-Element Method

Uday K. Khankhoje, Jakob J. van Zyl, *Fellow, IEEE*, and Thomas A. Cwik, *Fellow, IEEE*

***Abstract*—A 2-D vector-element-based finite-element method (FEM) is used to calculate the radar backscatter from 1-D bare rough soil surfaces which can have an underlying heterogeneous substrate. Monte Carlo simulation results are presented for scattering at L-band ($\lambda = 0.24$ m). For homogeneous soils with rough surfaces, the results of FEM are compared with the predictions of the small perturbation method. In the case of heterogeneous substrates, soil moisture (and, hence, soil permittivity) is assumed to vary as a function of depth. In this case, the results of FEM are compared with those of the transfer matrix method for flat soil surfaces. In both cases, a good agreement is found. For homogeneous rough soils, it is found that polarimetric radar backscatter and copolarized phase difference have a nonlinear relationship with soil moisture. Finally, it is found that the nature of the soil moisture variation in the top few centimeters of the soil has a strong influence on the backscatter and, hence, on the inferred soil moisture content.**

***Index Terms*—Electromagnetic scattering by rough surfaces, finite-element methods (FEMs), Monte Carlo simulations, subsurface sensing.**

I. Introduction

SOIL moisture is a key parameter in numerous environmental studies, including hydrology and meteorology, as well as in agricultural applications. It also plays an important role in interactions between the land surface and the atmosphere, as well as in the partitioning of precipitation into runoff and ground water storage [1]. An accurate monitoring of soil moisture is important for several environmental issues, including water resource management in low-precipitation regions and flood risk management. Its importance is reflected in the fact that a current satellite mission, the Soil Moisture and Ocean Salinity mission [2], and an upcoming mission, the Soil Moisture Active/Passive mission [1], seek to monitor soil moisture on a global scale.

Manuscript received March 26, 2012; revised September 5, 2012; accepted October 7, 2012.

U. K. Khankhoje was with the National Aeronautics and Space Administration Jet Propulsion Laboratory, California Institute of Technology, Pasadena, CA 91109 USA. He is now with the Department of Electrical Engineering, University of Southern California, Los Angeles, CA 90089 USA (e-mail: uday@alumni.caltech.edu).

J. J. van Zyl and T. A. Cwik are with the National Aeronautics and Space Administration Jet Propulsion Laboratory, California Institute of Technology, Pasadena, CA 91109 USA (e-mail: jakob.j.vanzyl@jpl.nasa.gov; thomas.a.cwik@jpl.nasa.gov).

Color versions of one or more of the figures in this paper are available online at http://ieeexplore.ieee.org.

Digital Object Identifier 10.1109/TGRS.2012.2225431

It is well documented that return signals from synthetic aperture radar are affected by characteristics such as the surface roughness, correlation length, and dielectric constant of the soil [3]. Nevertheless, inverting these measurements for soil moisture remains a difficult task. This is partly due to the difference between the observed characteristics of radar measurements and theoretical models, in the presence of changing soil wetness. Most theoretical models of bare surface scattering assume an infinite half-space with a homogeneous dielectric constant. In practice, it is often observed—and soil physics [4] predicts—that, most often, soil moisture will vary with depth. The backscattering cross section for a layered medium with a rough interface has been studied in [5] and [6]. An analytic method was derived to calculate the bistatic-scattering coefficient from an N-layered medium with slightly rough interfaces [5], where the electromagnetic waves in each layer are expressed in terms of an infinite number of angular spectral components. A small perturbation method (SPM) approach is used to calculate the scattered wave, which is appropriate for the scattering calculation for a low-frequency radar system. The problem of a varying moisture profile was also investigated by Le Morvan *et al.* [7] who modeled the varying profile with three layers of homogeneous dielectric constants. An effective dielectric constant was then calculated to be used in the Integral Equation Method (IEM) model to simulate the backscatter from the total system.

The objective of this paper is to develop numerical simulations to demonstrate how soil moisture profiles impact radar backscatter. Scattering from a 2-D soil body, i.e., comprising a 1-D rough surface given by $z = f(x)$, is numerically calculated using the FEM, removing the limitations on surface roughness for those approximations based on the SPM. The calculation is rigorous and solves for the scattering fields without having to approximate the subsurface profile by a layered structure, a key approximation made in the analytic methods described earlier. Earlier approaches that used the 2-D FEM to compute rough surface scattering [8], [9] had to contend with limited computational resources and hence simulated short surface lengths ($\approx 20\lambda$). To compensate, a periodic boundary condition was employed along the surface direction. This approach, which uses a plane wave excitation, leads to an infinite series of Floquet modes, and appropriate mode filtering must be performed to get the scattered fields. In more recent approaches on the subject [10], including the present, it is possible to simulate much longer surfaces ($\geq 70\lambda$) allowing for realistic

simulations of rough surfaces, particularly in the cases where surface correlation lengths are large. This is accomplished by applying absorbing boundary conditions (ABCs) all along the boundary and using a tapered wave excitation. Further details follow in subsequent sections.

It is instructive to compare scattering from 1-D and 2-D surfaces. For isotropically rough surfaces, this paper finds that 1-D surfaces scatter qualitatively in the same manner as 2-D surfaces [3], in the sense that the same trends in radar backscatter are seen as a function of surface roughness, correlation length, soil dielectric constant, and incidence angle. For anisotropic surfaces, it is not possible to accurately capture the scattering geometry with a 1-D surface, and in such cases, the use of a 2-D surface is inevitable. The order of magnitude lower computational costs in simulating 1-D surfaces over 2-D surfaces offer a convenient method to explore various scattering geometries for a given problem at hand.

The structure of this paper is as follows. First, the FEM is briefly described, followed by a discussion of the assumptions made and the numerical issues encountered. The results of FEM are then compared with those of the SPM for scattering from a rough surface (with roughness parameters such that the SPM results are applicable). After a discussion of the main sources of error in the FEM, results for scattering from a rougher surface are presented. The behavior of backscatter and copolarized phase difference as a function of soil moisture is discussed for a homogeneous soil layer with a rough surface. Finally, results for scattering from two different types of subsurface soil moisture profiles—wetting and drying—are illustrated. The transfer matrix method is used to validate the results for a perfectly flat soil. Rough soil is then considered, and it is shown that the observed backscatter varies substantially depending on the characteristics of the profile, even if the surface and deep layer moisture values remain constant.

II. FEM

A. Theory

In a 2-D vector-based finite-element method (FEM) that computes electromagnetic scattering, the starting point is the vector wave equation. The entire computational domain is tessellated into triangles, and the wave equation is enforced on each of these triangles, treating the field values on each triangle side as unknowns. Galerkin's method gives an approximate solution to a differential equation and provides the ability to discretize the problem at hand. Using Galerkin's testing with a test vector $\vec{T}$ gives the following weak form of the wave equation:

$$\int\int_{\Omega} \vec{T}(\vec{r}) \cdot \left[\nabla \times \left(\frac{1}{p(\vec{r})} \nabla \times \vec{U}(\vec{r}) \right) - k_0^2 q(\vec{r}) \vec{U}(\vec{r}) \right] dS = 0 \quad (1)$$

where $\vec{U}$ is the field in the $x-z$ plane; in the case of transverse magnetic (TM) polarization, $\vec{U}$ is the magnetic field $\vec{H}$, $p = \epsilon_r$, and $q = \mu_r$, whereas in the case of transverse electric (TE) polarization, $\vec{U}$ is the electric field $\vec{E}$, $p = \mu_r$ and $q = \epsilon_r$, with ϵ_r and μ_r being the relative permittivity and permeability, respectively, k_0 is the magnitude of the free-space wave vector, and Ω is the computational domain, depicted by the gray-shaded region in Fig. 1 and bounded by the mesh boundaries Γ_a and Γ_s in the same figure. After the use of appropriate vector identities and the Green's theorem, the aforementioned equation is transformed into a form suitable for numerical computation [11]

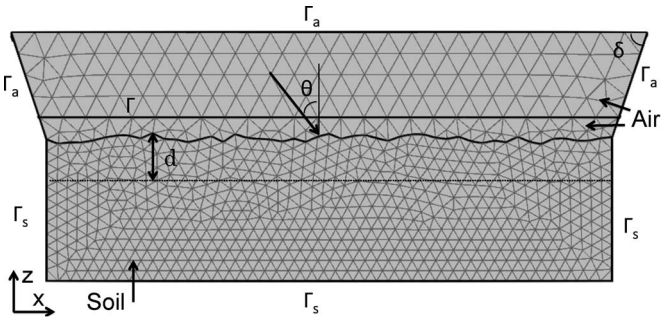

Fig. 1. Schematic showing tessellated computational domain. Γ_a and Γ_s denote the domain boundaries in air and soil, respectively. The straight line Γ denotes the integration contour from which the RCS is calculated (0.6λ above the mean soil–air interface). The field is incident at an angle θ, and δ is chosen such that any specularly reflected wave hits the horizontal portion of Γ_a (2.5λ above the mean soil–air interface) before hitting the side boundaries. For heterogeneous soil, d is the distance in which the soil displays heterogeneity in moisture, measured from the peak of the rough surface, after which the moisture is assumed to be constant. In this paper, $\theta = 40°$, $\delta = 45°$, the soil length is 70λ, and depth is 3.5λ, with $\lambda = 0.24$ m.

$$\int\int_{\Omega} \left[(\nabla \times \vec{T}) \cdot \left(\frac{1}{p} \nabla \times \vec{U} \right) - k_0^2 q \vec{T} \cdot \vec{U} \right] dS = \oint_{\Lambda} \vec{T} \times \left(\frac{1}{p} \nabla \times \vec{U} \right) \cdot \hat{n} dl \quad (2)$$

where Λ is the domain boundary and $\hat{n}$ is the outward contour normal (the position coordinate $\vec{r}$ is dropped for convenience).

The first-order ABC [12] is applied on Λ. This condition is derived by enforcing no reflection from the incidence of a plane wave on a planar boundary. To first order, this approximates the physical condition of the scattered field $\vec{U}_s$, being purely outgoing at the domain boundary

$$(\nabla \times \vec{U}_s) \times \hat{n} = jk_0 \cos\theta \left(\hat{n} \times (\hat{n} \times \vec{U}_s) \right) \quad (3)$$

where θ is the angle between the incident wave vector and boundary normal $\hat{n}$. Applying (3) (with θ typically set to 90°) to the right-hand side of (2) allows for the FEM system of equations to be solved.

B. Implementation

1) Incident Field: To implement the FEM system of equations, an incident field[1] tapered to have a low amplitude near the surface corners is chosen. Of course, such a field must also satisfy the wave equation in free space. The so-called Thorsos taper [13] has such a property and is given by [14]

$$\vec{U}_i(\vec{r}) = \exp\left\{ -j\vec{k}_0 \cdot \vec{r}[1 + w(\vec{r})] - \left[\frac{(x + z\tan\theta_i)^2}{g^2} \right] \right\} \hat{y} \quad (4)$$

[1]The implicit time harmonic convention is $e^{j\omega t}$.

where $\vec{k}_0$ is the incident wave vector in vacuum, θ_i is the incident angle defined w.r.t. the upward normal in a counterclockwise sense, $\vec{r} = (x, z)$ is the position vector (with the center of the soil surface being taken as the origin), and $w(\vec{r}) = 2\{[x + z\tan\theta_i]^2/g^2 - 1\}/(k_0 g\cos\theta_i)^2$. Here, g is the beam half waist on the surface. Provided that $k_0 g\cos\theta_i \gg 1$, the aforementioned equation satisfies the wave equation to order $1/(k_0 g\cos\theta_i)^2$, which, by appropriate choice of g, can be a very reasonable approximation. As reported by Thorsos, it is sufficient to have $g = L/4$, where L is the lateral length of the soil surface. A further detailed study [15] also showed that $g_{\min} = 6\lambda_0/(\cos\theta_i)^{1.5}$.

2) Application of ABC: The following are a few important points that must be made about the semi-infinite nature of the soil and the application of the ABC on the mesh boundaries.

1) In the free-space part of the domain, the scattered field is calculated by subtracting from the total field $\vec{U}$ the field in the absence of any scatterer (i.e., the known in-plane incident field $\vec{U}_{i\perp}$), giving $\vec{U}_s = \vec{U} - \vec{U}_{i\perp}$. The ABC given by (3) is applied on the contour Γ_a (see the mesh schematic in Fig. 1) to the scattered field. It is in this manner that the incident field enters into the FEM formulation via the boundary condition in (3).
2) In the soil part of the domain, it is not possible to decompose the total field in terms of an incident field and a purely outgoing scattered field[2], and hence, the ABC in (3) is applied on the contour Γ_s to the total field $\vec{U}$. This physically implies that the total field is purely outgoing at the mesh boundaries under the soil surface, which is a reasonable assumption.

The aforementioned modification makes it possible to accurately calculate scattering from a semi-infinite object with a relatively simple boundary condition.

3) Numerical Issues: To numerically solve (2), the domain is fractured into triangles using the De Launay algorithm while making sure that the maximum edge length satisfies $l_{\max} < \lambda/20$ (where λ is the wavelength in the medium) for an accurate solution. The first-order Whitney elements are used as basis functions for expanding the unknown field [11]. Using Galerkin's testing along with the ABC given in (3) gives a purely sparse matrix which is solved directly using the matrix MUltifrontal Massively Parallel sparse direct Solver (MUMPS) library [16]. The surface equivalence principle is applied on an (incomplete) contour (see contour Γ in Fig. 1) a small distance (0.6λ) above the mean soil surface to calculate the scattered far field, $U_f^s(r, \theta_s)$, in the direction θ_s, using which the radar scattering cross section (RCS) is computed. This RCS must be normalized appropriately [14] by the incident power on the surface, which gives the bistatic RCS as

$$\sigma_p(\theta_s, \theta_i) = \lim_{r\to\infty} \frac{2\pi r \left|U_f^s(r, \theta_s)\right|^2}{g\cos\theta_i\sqrt{\pi/2}} \tag{5}$$

where either $\{p = \text{TM}, U_f^s = E_y^{sf}\}$ or $\{p = \text{TE}, U_f^s = H_y^{sf}\}$.

[2]This is because the incident field is not a solution of Maxwell's equation in the soil region.

A typical FEM simulation of a single instance of rough soil with dimensions as mentioned in the caption of Fig. 1 involves solving for a sparse matrix of size ≈1 500 000 (for each polarization), which takes <2 min on a 3-GHz processor, consuming <2 GB of RAM.

III. Validation of FEM With SPM

There has been extensive research on the subject of rough surface scattering (see [17] and [18] for reviews). While the problem is not analytically tractable, there are a few semianalytical models that work successfully within a restricted range of roughness parameters. Among them is the first-order SPM, introduced by Rice in 1951 [19]. For the purpose of validation of the FEM code, Monte Carlo simulations of randomly rough 1-D surfaces with Gaussian and exponential correlation functions are considered, and the results are compared with the SPM predictions.

A Gaussian random surface is characterized by two parameters: the root-mean-square (rms) height of the rough surface h and the correlation length l. A derived quantity, the rms slope s, is often used for Gaussian surfaces and is given by $s = \sqrt{2}h/l$. The roughness spectrum $W(K)$ is the Fourier transform of the autocorrelation function and is given by $W(K) = h^2 l/(2\sqrt{\pi})\exp\{-(Kl/2)^2\}$, where K is the spatial wavenumber. On the other hand, the roughness spectrum for an exponentially correlated random surface is given by $W(K) = h^2 l/(\pi(1 + (Kl)^2))$ [20].

A. SPM Predictions

Expressed in terms of the electrical and statistical properties of a randomly rough 1-D surface with complex relative permittivity ϵ_r, the incoherent bistatic RCS σ according to first-order SPM [20], [21] is

$$\sigma_p = 8\pi k_0^3 \cos^2\theta_s \cos\theta_i |\alpha_p|^2 \times W\left(k_0[\sin\theta_s - \sin\theta_i]\right), \qquad p = \{\text{TM}, \text{TE}\} \tag{6}$$

where θ_i and θ_s are the incident and scattered angles, respectively, measured in a counterclockwise sense from the normal, and

$$\alpha_{\text{TM}} = -(\epsilon_r - 1)\beta$$

$$\alpha_{\text{TE}} = -(\epsilon_r - 1)\Big[\epsilon_r \sin\theta_i \sin\theta_s + \left\{(\epsilon_r - \sin^2\theta_i)(\epsilon_r - \sin^2\theta_s)\right\}^{1/2}\Big]\beta$$

$$\beta^{-1} = \left[\cos\theta_i + (\epsilon_r - \sin^2\theta_i)^{1/2}\right] \times \left[\cos\theta_s + (\epsilon_r - \sin^2\theta_s)^{1/2}\right].$$

B. Comparison of FEM With SPM

SPM is valid for relatively smooth surfaces, specifically [22] for surfaces with $kh < 0.3$ and $s < 17^\circ$. With this restriction

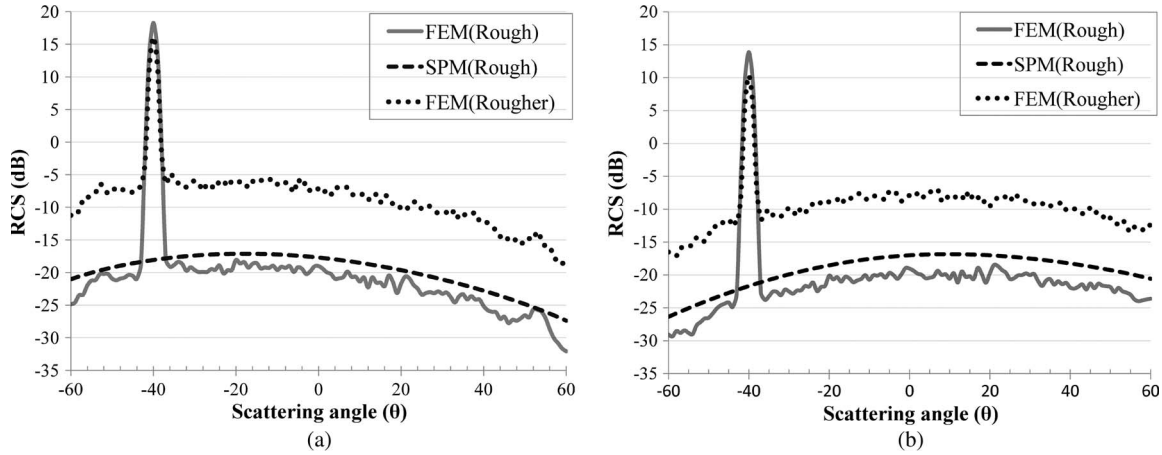

Fig. 2. Bistatic RCSs for (a) TM and (b) TE polarizations for $\lambda = 0.24$ m, incidence angle $\theta_i = 40^\circ$, and 15% soil moisture ($\epsilon_r = 6.940 - 1.814j$). The rough Gaussian-correlated soil surface has $kh = 0.1$ and $s = 5^\circ$, while rougher soil has $kh = 0.5$ and $s = 20^\circ$. Incoherent first-order SPM predictions for rough soil are also shown for comparison.

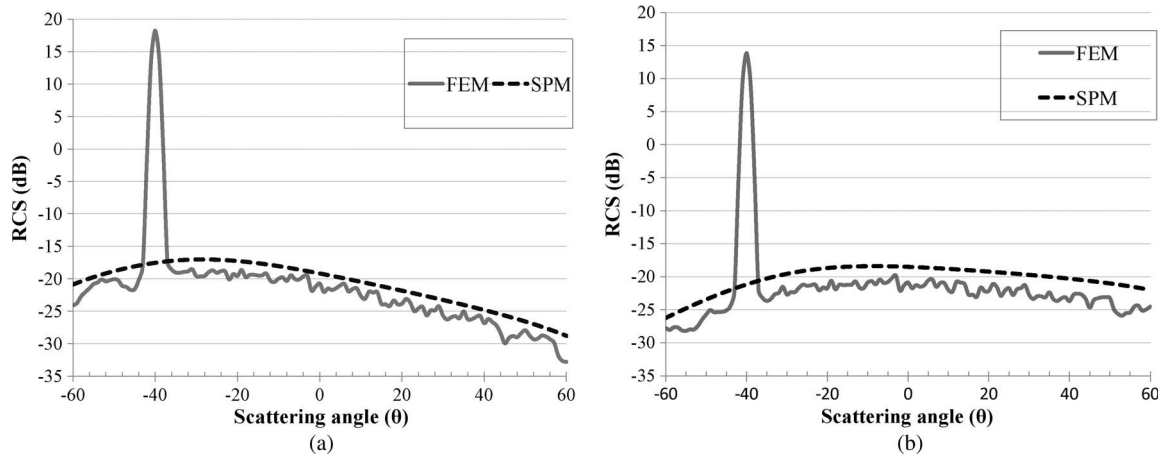

Fig. 3. Bistatic RCSs for (a) TM and (b) TE polarizations for $\lambda = 0.24$ m, incidence angle $\theta_i = 40^\circ$, and 15% soil moisture ($\epsilon_r = 6.940 - 1.814j$). The rough exponentially correlated soil surface has $kh = 0.1$ and $l = 16.3h$. Incoherent first-order SPM predictions for rough soil are also shown for comparison.

in place, the parameters that are chosen for comparing FEM results are $kh = 0.1$ and $s = 5^\circ$. Using an empirical microwave dielectric model for wet soil [23], the soil composition is chosen to be the silt loam soil with a volumetric moisture of $0.15\ \text{cm}^3 \cdot \text{cm}^{-3}$. In this model, the real and imaginary parts of the soil permittivity are quadratic functions of volumetric soil moisture mv. Specifically, $\epsilon_r(mv) = (2.201 + 26.406\ mv + 34.563\ mv^2) - (-0.141 + 11.820\ mv + 8.100\ mv^2)j$.

Random surface is generated using standard schemes that have been described previously by researchers [13], [24]. Monte Carlo simulations are then performed, and results are shown in Fig. 2 for the ensemble-averaged (coherent) RCS as a function of scattering angle for a fixed incidence angle $\theta_i = 40^\circ$ for a total of 100 instances of rough soil. A given soil surface is 70λ in length and is generated by connecting straight line points that are $\lambda/40$ apart, with $\lambda = 24$ cm. These are compared with the SPM predictions in Figs. 2 and 3, and an overall good agreement is observed. It must be noted that the FEM solution is coherent, while the SPM formula is only the incoherent field contribution; hence, it lacks the peak in the specular direction in these two figures.

In the case of Gaussian correlation surfaces, the FEM solution for rough soil with $kh = 0.1$ and $s = 5^\circ$ is found to be consistently lower than the SPM results by 1–3 dB for TM polarization and 2–4 dB for TE polarization, as seen in Fig. 2. The agreement in the case of exponentially correlated surfaces is found to be similar; the FEM solution for rough soil with the same rms height and correlation length as described earlier is found to be lower than the SPM results by 1–3 dB for TM polarization and 2–4 dB for TE polarization, as seen in Fig. 3. Recent work suggests that exponentially correlated soils better represent realistic soil surfaces [25]. However, since the main focus of this paper is to examine the effects of subsurface soil moisture variations on backscatter, the exact statistics of the surface are not very crucial, and Gaussian correlation surfaces are chosen.

C. Sources of Error in FEM

The section is concluded with a discussion of the dominant sources of error in the FEM computation.

1) Choice of basis functions for representing the fields: Recall that, in the TM case, $\vec{H}$ is expanded along a first-order basis in the computational plane $(x-z)$, and as a result, the electric field E_y (obtained by taking the curl of $\vec{H}$) is expanded along a zeroth-order basis (i.e., it is

piecewise constant). In the TE case, the roles of $\vec{E}$ and $\vec{H}$ are reversed. The soil body represents an electrical discontinuity, and the inability of the basis functions to model the corresponding fields accurately leads to error. The use of higher order basis functions [26] solves this problem. The computational costs of such an approach are slightly higher, but they are offset by the fact that the domain can be meshed in a relatively less dense manner.

2) Nonzero reflectivity of the vacuum ABC: Due to the nonexact behavior of the vacuum ABC, the scattered field gets reflected back to the soil surface by the vacuum ABC (contour Γ_a in Fig. 1). A popular approach to solve this problem is the use of perfectly matched layers to create nonreflective boundaries [27], [28]. Nevertheless, another approach is to go to a higher order ABC to reduce reflectivity [29]. As has been astutely observed in [30], it is necessary to go to the next order of basis functions *and* ABC in order to overcome the first two problems.
3) Numerical derivatives for calculating RCS: The far field is calculated by using the Green's integral theorem which requires the magnetic and electric currents on the contour Γ. In either polarization, one of the currents needs to be calculated by taking the numerical derivative of the other—a process that introduces its own error. This problem can be overcome by employing a coupled finite-element–boundary integral formulation [31]. While this method is exact, the computational disadvantage is that the sparse nature of the FEM matrix is lost.

IV. FEM Results for Rough Soil

In this section, the scattering properties of Gaussian rough surfaces will be presented, and wherever ensemble averages are mentioned, 100 instances of rough soil have been taken. Unless otherwise stated, the incidence angle is fixed at $\theta_i = 40^\circ$ and $\lambda = 0.24$ m.

A. Homogeneous Soil

First, silt loam soil with a volumetric moisture of 0.15 $\text{cm}^3 \cdot \text{cm}^{-3}$ is considered, and Fig. 2 shows the ensemble-averaged bistatic RCS as a function of scattering angle. As expected, the radar return is higher from a rougher soil as compared to that from a smoother soil. The roughness parameters $kh = 0.5$ and $s = 20^\circ$ fall outside the scope of the SPM, but it can be mentioned in passing that, in this case, SPM overestimates the RCS by 1–5 dB for TM polarization and 3–6 dB for TE polarization.

Next, ensemble-averaged radar backscatter is considered as a function of soil moisture. This can be seen in Fig. 4, which also shows logarithmic curves fitted to the data, i.e., $10\log(\sigma) = a\ \log(mv) + b$, where σ is the radar backscatter, a and b are fitting constants, and mv is the soil moisture (here expressed as $100\times$ volumetric soil moisture). It is indeed remarkable that the curves fit the data to such a high degree. It was found that logarithmic curves (with different parameters; see caption of Fig. 4) also fitted the data from scattering off the smoother Gaussian surface considered in the previous section ($kh = 0.1$ and $s = 5^\circ$).

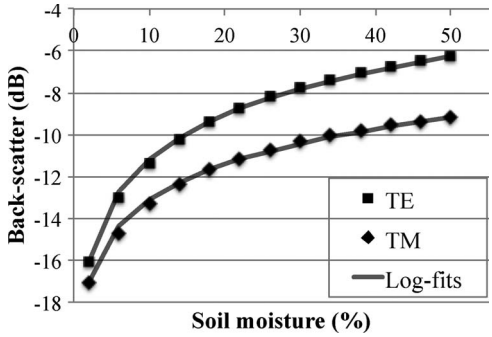

Fig. 4. Ensemble-averaged radar backscatter as a function of soil moisture (mv, expressed as a percentage) for rough Gaussian soil with $kh = 0.5$ and $s = 20^\circ$. The fitted curves are of the form $(a\ \log(mv) + b)$ with $a = 5.63$ and $b = -18.75$ for TM and $a = 7.02$ and $b = -18.19$ for TE. The fitting parameters for rough soil with $kh = 0.1$ and $s = 5^\circ$ (not plotted here) are $a = 5.52$ and $b = -31.79$ for TM and $a = 6.99$ and $b = -30.10$ for TE.

Many researchers have commented on the empirical relation between radar backscatter and soil parameters such as roughness, correlation statistics, and moisture [22], [32], [33]. These include linear and logarithmic relations between soil moisture and logarithmic backscatter. It is evident from the literature that there is no universal relation; rather, specific relations between moisture and backscatter exist, depending on the range of soil parameters. Furthermore, the aforementioned cited literature reports extensively on the relation between backscatter and soil roughness or incidence angle, while the relation between backscatter and soil moisture is limited to a few particular values of moisture content. It is in this light that the data obtained from a fully numerical technique, as in this paper, are useful in adding to the understanding of the relationship between backscatter and soil moisture.

Finally, the behavior of phase difference between the scattered far fields of the TM and TE polarizations, i.e., $\arg(E_y^{sf}) - \arg(H_y^{sf})$, is considered for single instances of "rough" ($kh = 0.1$ and $s = 5^\circ$) and "rougher" soil ($kh = 0.5$ and $s = 20^\circ$), respectively, and is shown graphically in Fig. 5. Like in the case of backscatter versus soil moisture (Fig. 4), the phase shows a nonlinear (and monotonically increasing) relation with moisture. Indeed, this behavior has been observed previously in experimental data [34], as well as predicted by semiempirical models [35].

B. Soil With Varying Moisture Content

In the next series of simulations, the radar backscatter from soil surfaces with varying moisture content in the top few centimeters (the distance marked d in Fig. 1) of the soil is considered.

Two types of moisture profiles are considered: first, a wetting profile where moisture decreases from 45% at the top to 25% at depth d and, second, a drying profile where moisture increases from 5% at the top to 25% at depth d. Two different functional forms for the profiles are considered: linear and exponential. In all cases, the soil moisture is constant below the depth d (i.e., below the dashed line in Fig. 1), and the overall profile is

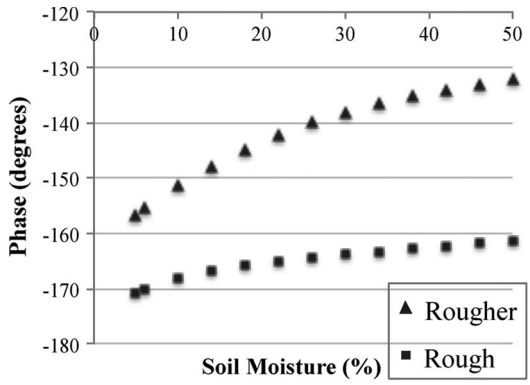

Fig. 5. Copolarized phase difference (TM − TE) as a function of soil moisture (expressed as a percentage) for single instances of "rough" ($kh = 0.1$ and $s = 5°$) and "rougher" soil ($kh = 0.5$ and $s = 20°$).

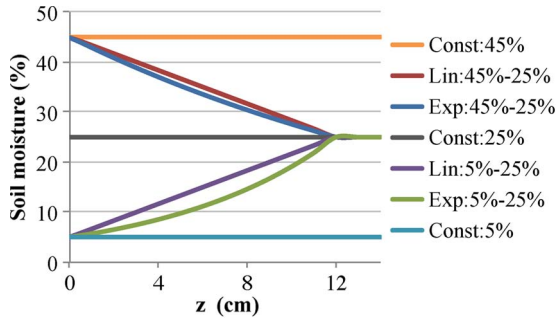

Fig. 6. Graphical representation of soil moisture variation (in percentage) as a function of soil depth z in centimeters, when the depth to constant soil moisture d is chosen to be 12 cm. For any given rough surface, the vertical moisture variation is chosen to start from the highest peak of the rough surface.

a continuous function of moisture. A graphical representation of the soil moisture variation as a function of soil depth can be seen in Fig. 6. It must be mentioned that the soil moisture profiles described earlier are not derived from hydrodynamic considerations (see [4] for a discussion) and do not correspond, in a quantitative way, to realistic moisture profiles. Instead, the idea is to examine the influence on backscatter of a wetting or a drying soil moisture profile for some simple functional forms.

First, the results of transfer matrix theory are compared to FEM results. For this, the power reflectivity for normal incidence of a plane wave on a perfectly flat infinitely long surface is considered. This problem has an analytical solution, which is computed by using transfer matrix theory. In this theory, the reflection and transmission properties of a slab (possibly infinite) of material with homogeneous dielectric properties are first calculated by applying the electric and magnetic field boundary conditions. The properties of a larger slab are then calculated by cascading the results of the constituent slabs. In this case, the dielectric properties of flat soil are treated in a piecewise constant manner, and a total of 1000 slabs are used for any given value of d, the distance to constant soil moisture. The largest distance considered here is $d = 8$ cm, which translates to the dielectric properties being constant over a distance of $\lambda/3000$, which is a very reasonable assumption. Using a plane wave incident field, FEM is then used to calculate the reflectivity for each case, and as can be seen in Fig. 7, there

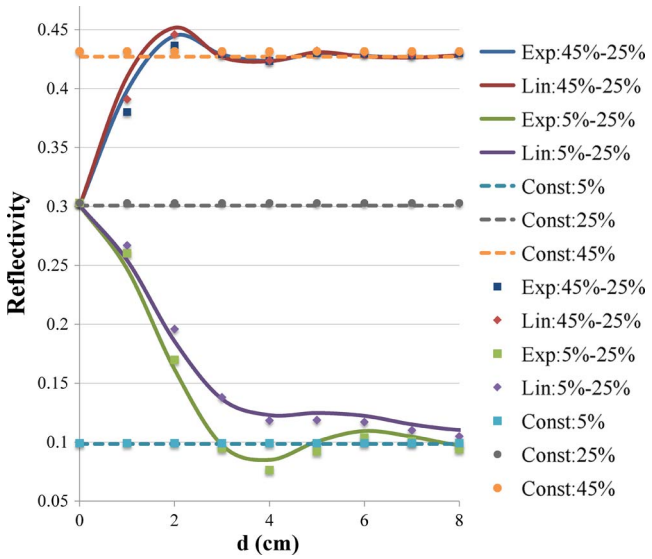

Fig. 7. Power reflectivity as a function of the depth to constant soil moisture for normal incidence on a perfectly smooth soil surface. The solid and dashed lines represent data from transfer matrix theory, while the discrete points represent data from FEM simulations. In the legend, "Exp : $X\%-Y\%$" and "Lin : $X\%-Y\%$" represent exponential and linear moisture profiles, varying in that functional form from X at the top to $Y\%$ at depth d and constant at $Y\%$ below d. "Const : $Z\%$" refers to soil having constant $Z\%$ moisture everywhere. See Fig. 6 for a graphical representation of the various soil moisture profiles.

is an excellent agreement with transfer matrix theory, with the worst case error being less than 5%.

Next, FEM is applied to calculate scattering from rough soil at an incidence angle of $\theta_i = 40°$. From a computational point of view, it is prohibitively time consuming to take ensemble averages for each value of d in all possible moisture profiles. Instead, a single instance of a rough soil is considered for each of the two soil types mentioned in this paper. Data from rough soil with $kh = 0.1$ and $s = 5°$ are shown in Fig. 8, while the rougher case of $kh = 0.5$ and $s = 20°$ is shown in Fig. 9. To provide suitable reference points, the cases of constant soil moisture (for $mv = 5\%$, 25%, and 45%) are plotted simultaneously.

The following observations on wetting profiles are described. The asymptotic behavior is on expected lines; for $d \to 0$, the RCS approaches the RCS of the soil with constant $mv = 25\%$ (the dominant moisture content in this case). For $d > \lambda$, the RCS approaches the other asymptote (of $d \to \infty$, soil with constant $mv = 45\%$) relatively sooner (i.e., for smaller values of d) in the case of the smoother soil. The behavior for intermediate d is quite different between the two types of soil and between the two polarizations. For smoother soil, the TM polarization displays a counterintuitive phenomena of having an RCS greater than the RCS of constant $mv = 45\%$ (for some values of d), even though no part of the soil has $mv > 45\%$. Surely, interference effects are responsible for this behavior. In fact, this effect was already seen in the case of a perfectly flat soil (see Fig. 7) when the reflectivity for certain intermediate values of d exceeded that of a constant soil moisture. If, in the process of inverting the RCS to obtain the soil moisture, the assumption of soil having constant moisture is made, the aforementioned observation would lead to the erroneous conclusion

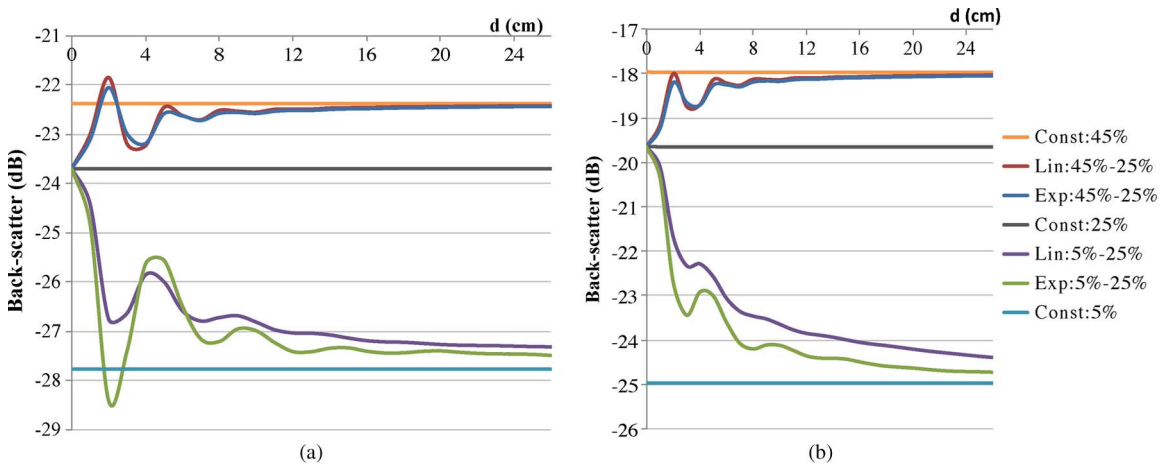

Fig. 8. Impact on backscatter of soil moisture variation in top d centimeters of the soil that has roughness parameters $kh = 0.1$ and $s = 5^\circ$ for (a) TM and (b) TE polarizations (incidence angle is $\theta_i = 40^\circ$). The legend has the same meaning as in Fig. 7.

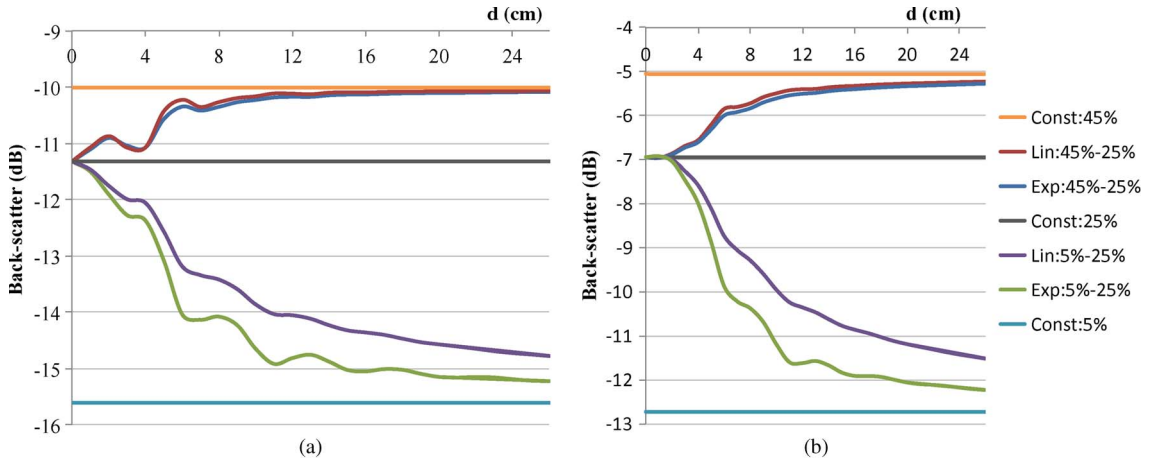

Fig. 9. Impact on backscatter of soil moisture variation in top d centimeters of the soil that has roughness parameters $kh = 0.5$ and $s = 20^\circ$ for (a) TM and (b) TE polarizations (incidence angle is $\theta_i = 40^\circ$). The legend has the same meaning as in Fig. 7.

of the soil being wetter than the wettest parts of the constituent soil! This behavior is not observed in the case of rougher soil, presumably because interference effects are damped out by the rougher soil. Finally, the behavior of the linear and exponential profiles is practically indistinguishable.

The following observations on drying profiles are reported. The asymptotic behavior is qualitatively the same as for wetting profiles, but it is found that the RCS approaches the asymptote of $d \to \infty$ at much larger values of d. Judging by the slope of the curves in the aforementioned figures, it is clear that the RCS is more sensitive to d in the case of a drying profile. For intermediate values of d, the behavior is analogous to the behavior of the wetting profiles. Again, (only) in the smoother soil, the TM polarization displays a similar counterintuitive phenomena, where, for certain values of d, the RCS is lower than the RCS of the soil with constant $mv = 5\%$. It must be noted that this behavior is seen only in the case of an exponential—not linearly—drying profile.

An important question that comes up is whether the aforementioned seen effects hold only for a single instance, or are also seen in ensemble behavior. Ensemble simulations were performed for a select few profiles, and it was found that the ensemble behavior is essentially the same, with a few differences in the exact values of RCS. The asymptotic behavior is identical, and the interference effect seen earlier is also observed in the case of the ensemble.

The implications of the results of this section are that the variations in soil moisture in the topmost wavelength-long part of the soil have profound impacts on the inferred soil moisture content.

V. Conclusion

In this paper, the power of the FEM in modeling electromagnetic scattering off complex geometries has been demonstrated. Most of the restrictions that accompany the use of semianalytical methods are eliminated by this method. Three key issues are reported in this paper: one, the nonlinear behavior of backscatter as a function of soil moisture; two, the nonlinear behavior of copolarized phase difference as a function of soil moisture; and three, the impact of variable subsurface soil moisture on backscatter for different cases of wetting and drying soils.

Due to the method being 2-D, the computational requirements in terms of processor time and memory usage are very modest. The use of a similar method in three dimensions (using a commercial software) has also been reported recently [36].

In the latter case, simulation times run into hours, whereas the method described in this paper runs on the order of minutes. The great advantage here is that many different kinds of subsurface profiles can be simulated in a reasonable time frame and confirmed with the use of Monte Carlo methods. It is possible to vary not just the soil moisture but other variables of interest as well, such as soil salinity, solute content, or even a heterogeneity in soil type. In fact, a restriction to soil is not necessary, and ocean phenomena can also be studied with this method. On the other hand, owing to the method being 2-D, it is not possible to calculate any cross-polarization quantities.

ACKNOWLEDGMENT

The authors would like to thank Dr. Y. Kim and Dr. S. Saatchi, Jet Propulsion Laboratory (JPL), for useful discussions on rough surface scattering as well as two anonymous reviewers for very helpful reviews. The authors would also like to thank the members of the Soil Moisture Active Passive Science Data System team at JPL for providing the computational resources that enabled this research. This research was carried out at JPL, California Institute of Technology, under a contract with the National Aeronautics and Space Administration.

REFERENCES

[1] D. Entekhabi, E. Njoku, P. O'Neill, K. Kellogg, W. Crow, W. Edelstein, J. Entin, S. Goodman, T. Jackson, J. Johnson, J. Kimball, J. Piepmeier, R. Koster, N. Martin, K. McDonald, M. Moghaddam, S. Moran, R. Reichle, J. Shi, M. Spencer, S. Thurman, L. Tsang, and J. Van Zyl, "The Soil Moisture Active Passive (SMAP) mission," *Proc. IEEE*, vol. 98, no. 5, pp. 704–716, May 2010.

[2] Y. Kerr, P. Waldteufel, J. Wigneron, J. Martinuzzi, J. Font, and M. Berger, "Soil moisture retrieval from space: The Soil Moisture and Ocean Salinity (SMOS) mission," *IEEE Trans. Geosci. Remote Sens.*, vol. 39, no. 8, pp. 1729–1735, Aug. 2001.

[3] S. Huang, L. Tsang, E. G. Njoku, and K.-S. Chen, "Backscattering coefficients, coherent reflectivities, emissivities of randomly rough soil surfaces at L-band for SMAP applications based on numerical solutions of Maxwell equations in three-dimensional simulations," *IEEE Trans. Geosci. Remote Sens.*, vol. 48, no. 6, pp. 2557–2568, June 2010.

[4] T. J. Marshall, J. W. Holmes, and C. W. Rose, *Soil Physics*, 3rd ed. Cambridge, U.K.: Cambridge Univ. Press, 1996.

[5] A. Tabatabaeenejad and M. Moghaddam, "Bistatic scattering from three-dimensional layered rough surfaces," *IEEE Trans. Geosci. Remote Sens.*, vol. 44, no. 8, pp. 2102–2114, Aug. 2006.

[6] C.-H. Kuo and M. Moghaddam, "Electromagnetic scattering from multilayer rough surfaces with arbitrary dielectric profiles for remote sensing of subsurface soil moisture," *IEEE Trans. Geosci. Remote Sens.*, vol. 45, no. 2, pp. 349–366, Feb. 2007.

[7] A. Le Morvan, M. Zribi, N. Baghdadi, and A. Chanzy, "Soil moisture profile effect on radar signal measurement," *Sensors*, vol. 8, no. 1, pp. 256–270, Jan. 2008.

[8] S. H. Lou, L. Tsang, and C. H. Chan, "Application of the finite element method to Monte Carlo simulations of scattering of waves by random rough surfaces: Penetrable case," *Waves Random Media*, vol. 1, no. 4, pp. 287–307, Oct. 1991.

[9] K. Pak, L. Tsang, L. Li, and C. H. Chan, "Combined random rough surface and volume scattering based on Monte Carlo simulations of solutions of Maxwell's equations," *Radio Sci.*, vol. 28, no. 3, pp. 331–338, May 1993.

[10] P. Liu and Y.-Q. Jin, "Numerical simulation of bistatic scattering from a target at low altitude above rough sea surface under an EM-wave incidence at low grazing angle by using the finite element method," *IEEE Trans. Antennas Propag.*, vol. 52, no. 5, pp. 1205–1210, May 2004.

[11] J. Jin, *The Finite Element Method in Electromagnetics*, 2nd ed. Hoboken, NJ: Wiley, 2002.

[12] A. Bayliss, M. Gunzburger, and E. Turkel, "Boundary conditions for the numerical solution of elliptic equations in exterior regions," *SIAM J. Appl. Math.*, vol. 42, no. 2, pp. 430–451, Apr. 1982.

[13] E. I. Thorsos, "The validity of the Kirchhoff approximation for rough surface scattering using a Gaussian roughness spectrum," *J. Acoust. Soc. Amer.*, vol. 83, no. 1, pp. 78–92, Jan. 1988.

[14] D. A. Kapp and G. S. Brown, "A new numerical method for rough-surface scattering calculations," *IEEE Trans. Antennas Propag.*, vol. 44, no. 5, pp. 711–721, May 1996.

[15] H. Ye and Y.-Q. Jin, "Parameterization of the tapered incident wave for numerical simulation of electromagnetic scattering from rough surface," *IEEE Trans. Antennas Propag.*, vol. 53, no. 3, pp. 1234–1237, Mar. 2005.

[16] P. R. Amestoy, I. S. Duff, J. Koster, and J.-Y. L'Excellent, "A fully asynchronous multifrontal solver using distributed dynamic scheduling," *SIAM J. Matrix Anal. Appl.*, vol. 23, no. 1, pp. 15–41, Oct. 2001.

[17] K. Warnick and W. Chew, "Numerical simulation methods for rough surface scattering," *Waves Random Media*, vol. 11, no. 1, pp. 1–30, Jan. 2001.

[18] T. Elfouhaily and C.-A. Guérin, "A critical survey of approximate scattering wave theories from random rough surfaces," *Waves Random Media*, vol. 14, no. 4, pp. R1–R40, Oct. 2004.

[19] S. O. Rice, "Reflection of electromagnetic waves from slightly rough surfaces," *Commun. Pure Appl. Math.*, vol. 4, no. 2/3, pp. 351–378, Aug. 1951.

[20] X. Gu, L. Tsang, and H. Braunisch, "Modeling absorption of rough interface between dielectric and conductive medium," *Micro. Opt. Technol. Lett.*, vol. 49, no. 1, pp. 7–13, Jan. 2007.

[21] C. Chan, L. Tsang, and Q. Li, "Monte Carlo simulations of large-scale one-dimensional random rough-surface scattering at near-grazing incidence: Penetrable case," *IEEE Trans. Antennas Propag.*, vol. 46, no. 1, pp. 142–149, Jan. 1998.

[22] J. V. Zyl and Y. Kim, *JPL Space Science and Technology Series: Synthetic Aperture Radar Polarimetry*. Hoboken, NJ: Wiley, 2011.

[23] M. Hallikainen, F. Ulaby, M. Dobson, M. El-Rayes, and L.-K. Wu, "Microwave dielectric behavior of wet soil-Part 1: Empirical models and experimental observations," *IEEE Trans. Geosci. Remote Sens.*, vol. GE-23, no. 1, pp. 25–34, Jan. 1985.

[24] E. Jakeman and K. Ridley, *Modeling Fluctuations in Scattered Waves*, vol. 1. New York: Taylor & Francis, 2006.

[25] Q. Li, M. Y. Xia, L. Tsang, L. Zhou, C. H. Chan, and Z. X. Li, "Rough Surface Scattering: Numerical Simulations and Applications in Microwave Remote Sensing," in *Encyclopedia of RF and Microwave Engineering*. Hoboken, NJ: Wiley, 2005, pp. 4549–4584.

[26] R. Graglia, D. Wilton, and A. Peterson, "Higher order interpolatory vector bases for computational electromagnetics," *IEEE Trans. Antennas Propag.*, vol. 45, no. 3, pp. 329–342, Mar. 1997.

[27] J. Berenger, "A perfectly matched layer for the absorption of electromagnetic waves," *J. Comput. Phys.*, vol. 114, no. 2, pp. 185–200, Oct. 1994.

[28] J. Wu, D. Kingsland, J. Lee, and R. Lee, "A comparison of anisotropic PML to Berengers PML and its application to the finite-element method for EM scattering," *IEEE Trans. Antennas Propag.*, vol. 45, no. 1, pp. 40–50, Jan. 1997.

[29] J. P. Webb and V. N. Kanellopoulos, "Absorbing boundary conditions for the finite element solution of the vector wave equation," *Microw. Opt. Technol. Lett.*, vol. 2, no. 10, pp. 370–372, Oct. 1989.

[30] M. Botha and D. Davidson, "Rigorous, auxiliary variable-based implementation of a second-order ABC for the vector FEM," *IEEE Trans. Antennas Propag.*, vol. 54, no. 11, pp. 3499–3504, Nov. 2006.

[31] T. Cwik, C. Zuffada, and V. Jamnejad, "Modeling three-dimensional scatterers using a coupled finite element-integral equation representation," *IEEE Trans. Antennas Propag.*, vol. 44, no. 4, pp. 453–459, Apr. 1996.

[32] P. Dubois, J. V. Zyl, and T. Engman, "Measuring soil moisture with imaging radars," *IEEE Trans. Geosci. Remote Sens.*, vol. 33, no. 4, pp. 915–926, Jul. 1995.

[33] Y. Oh, K. Sarabandi, and F. Ulaby, "An empirical model and an inversion technique for radar scattering from bare soil surfaces," *IEEE Trans. Geosci. Remote Sens.*, vol. 30, no. 2, pp. 370–381, Mar. 1992.

[34] Y. Lasne, P. Paillou, A. Freeman, T. Farr, K. Mcdonald, G. Ruffié, J.-M. Malézieux, and B. Chapman, "Study of hypersaline deposits and analysis of their signature in airborne and spaceborne SAR data: Example of Death Valley, California," *IEEE Trans. Geosci. Remote Sens.*, vol. 47, no. 8, pp. 2581–2598, Aug. 2009.

[35] Y. Lasne, P. Paillou, T. August-Bernex, G. Ruffié, and G. Grandjean, "A phase signature for detecting wet subsurface structures using polarimetric L-band SAR," *IEEE Trans. Geosci. Remote Sens.*, vol. 42, no. 8, pp. 1683–1694, Aug. 2004.

[36] H. Lawrence, F. Demontoux, J. Wigneron, P. Paillou, T. Wu, and Y. Kerr, "Evaluation of a numerical modeling approach based on the finite-element method for calculating the rough surface scattering and emission of a soil layer," *IEEE Geosci. Remote Sens. Lett.*, vol. 8, no. 5, pp. 953–957, Sep. 2011.

Uday K. Khankhoje received the B.Tech. degree in electrical engineering from the Indian Institute of Technology Bombay, Mumbai, India, in 2005 and the M.S. and Ph.D. degrees in electrical engineering from the California Institute of Technology (Caltech), Pasadena, in 2010.

Previously, he was a Postdoctoral Scholar with the Jet Propulsion Laboratory, Caltech. He is a Postdoctoral Scholar with the Ming Hsieh Department of Electrical Engineering, University of Southern California, Los Angeles. His research interests include the application of computational electrodynamics to radar remote sensing. In the past, he has worked on the design, electromagnetic modeling, and fabrication of semiconductor optical resonators to conduct experiments in cavity quantum electrodynamics.

Jakob J. van Zyl (S'85–M'86–SM'95–F'99) received the B.Eng. degree (*cum laude*) in electronics engineering from the University of Stellenbosch, Stellenbosch, South Africa, and the M.S. and Ph.D. degrees in electrical engineering from the California Institute of Technology (Caltech), Pasadena.

From 1997 to 2001, he was an Adjunct Faculty Member with the Department of Aerospace and Mechanical Engineering, University of Southern California, Los Angeles, where he taught the class "Remote Sensing Systems from Space." Since 1986, he has been with the National Aeronautics and Space Administration Jet Propulsion Laboratory (JPL), Caltech, where he held positions of increasing responsibility in the synthetic aperture radar program, managed the Radar Science and Engineering Section, the Earth Science Flight Missions and Experiments Office, and the Focused Physical Oceanography and Solid Earth Program Office, was the Director and then the Deputy Director in 2002 for Astronomy and Physics Directorate, is the Associate Director of Project Formulation and Strategy and the Jet Propulsion Laboratory, and since 2002 has been teaching the class "Physics and Techniques of Remote Sensing" at Caltech.

Thomas A. Cwik (S'79–M'79–SM'94–F'01) received the B.S., M.S., and Ph.D. degrees from the University of Illinois, Urbana-Champaign, in 1979, 1981, and 1986, respectively.

He was with the Very Large Array, National Radio Astronomy Observatory, Socorro NM, building low-frequency feedhorns; with the Joint Institute for Laboratory Astrophysics, National Bureau of Standards (now National Institute of Standards and Technology), Boulder, CO, building a three-wavelength geodimeter; and upon completion of his Ph.D. degree, with the Electronics Research Laboratory, Norwegian Institute of Technology, Trondheim, Norway, where, as a Postdoctoral Fellow, he developed an analysis of shaped reflector antennas at and near caustic field locations. He is an Affiliate Professor with the Department of Electrical Engineering, University of Washington, Seattle. He was a Fellow at the Texas Institute for Computational and Applied Mathematics, Austin, in 1997. He is a Principal Member and Manager of the National Aeronautics and Space Administration Technology Program with the NASA Jet Propulsion Laboratory (JPL), California Institute of Technology, Pasadena, where, in this role, he is the key to strategic planning and oversight of science and technology research and development. Previous to being a manager of the NASA Technology Program, he was an Associate Chief Technologist with JPL, previous to which, he managed the Earth Science Instruments and Technology Office at JPL.

Dr. Cwik was a recipient of the IEEE Gordon Bell Prize Finalist Award in 1992 for parallel processing research.